Available online at www.sciencedirect.com
ScienceDirect
Journal of Power Sources 164 (2007) 278–283
JOURNAL OF POWER SOURCES
www.elsevier.com/locate/jpowsour

Short communication

Properties of Fe–Cr based alloys as interconnects in a solid oxide fuel cell

Minfang Han [a,b,*], Suping Peng [a,c], Zhongli Wang [a,b], Zhibin Yang [a,b], Xin Chen [a,b]

[a] Union Research Center of Fuel Cell, China University of Mining & Technology, Beijing 100083, PR China
[b] School of Chemical & Environmental Engineering, China University of Mining & Technology, Beijing 100083, PR China
[c] National Key Laboratory of Coal Sources, China University of Mining & Technology, Beijing 100083, PR China

Received 24 July 2006; received in revised form 5 October 2006; accepted 6 October 2006
Available online 15 November 2006

Abstract

Four kinds of Fe-Cr based alloys were investigated in this paper. The thermal expansion coefficients of the four samples at 900 °C were between 11 and 13 × 10^{-6} cm cm^{-1} K^{-1}. The coefficient of sample Fe-Cr-4 was close to that of yttrium stabled zirconia (YSZ). Compared with traditional alloys, the new type of Fe–Cr based alloys had decreased thermal expansion coefficients. With the increase of oxidation time, the weight gains of Fe-Cr-1 and -4 tended to be stable. The oxide scale of $3Cr_2O_3{\cdot}Fe_2O_3$ formed on the surface of Fe-Cr-1 and -4 was inactive and helpful to restrain the samples from internal oxidation. But the $FeCr_2O_4$ and $Cr_{1.3}Fe_{0.7}O_3$ formed on the surface of Fe-Cr-2 and -3 had no such effective restraint mechanism. Fe-Cr-1 and -4 exhibited better oxidation resistance than Fe-Cr-2 and -3.

PACS: 81.05.Bx; 82.47.Ed

Keywords: SOFC; Interconnect; Fe–Cr alloys; Thermal expansion properties; Oxidation resistance properties

1. Introduction

As a new type of power generating system, solid oxide fuel cell (SOFC) attracts more attention [1–7]. Interconnects in SOFCs provide the electrical contact between the anodes and cathodes of adjacent cells as well as separation of the air and fuel supplies. Accordingly, interconnects must be good electronic conductors (with thermal expansion properties matched to YSZ electrolyte and the electrodes materials) and must also retain good contact in both oxidizing and reducing atmospheres. Thus, interconnects must seal, be refractory and have good oxidation resistance and electrical conductivity.

Ceramic interconnects like $La_{1-x}(Sr,Ca)_xCrO_3$ have been used in traditional SOFCs [8–12]. However, they are difficult to fabricate and use on a large scale. The traditional metallic interconnects like stainless steel (i.e. Crofer22 APU, SUS430, X10CrAl18 and ZMG232) [13,14] or Inconel heat-resistant alloys (i.e. Incone1600, Incone1601, Incone1625, Incone1657, Incone1718, Ni20Cr and Hastelloy X), though mechanically advantageous, not only deform due to their high thermal expansion coefficients at high temperatures, but also have greater electrical resistance caused by the oxide scales on their surfaces [15].

Therefore, it is required to develop a new type of alloy with properties of oxidation resistance, high-temperature electrical conductivity, high temperature resistance and thermal expansion coefficients matched to the YSZ electrolyte (10–12 × 10^{-6} cm cm^{-1} K^{-1}) so as to extend life-span.

2. Experimental

The studied materials were Fe–Cr based alloys containing a small amount of microelements (such as Ni, Al, Si and Zr) and with limited amounts of C, P and S. The prepared compositions are listed in the Table 1 [16]. Fe–Cr based alloys were prepared by the following process. By conventional melting techniques, the theoretically designed compositions were melted and molded into ingots. After forging and rolling, the alloys were sectioned according to the required size and shape. The thermal expansion properties of the alloys were measured using a Netzsch Dil402C Thermal Analyzer. The behavior of electrical conductivity at different temperatures was observed by a four-probe method

* Corresponding author. Tel.: +86 10 62341427; fax: +86 10 62331344.
E-mail address: hanminfang@sina.com (M. Han).

0378-7753/$ – see front matter © 2006 Elsevier B.V. All rights reserved.
doi:10.1016/j.jpowsour.2006.10.039

Table 1
Composition of Fe–Cr alloys

No.	Cr	Si	Al	Zr	Ni	C	P	S
1	20	0.42	0.24	0.24	0.29	0.026	0.012	0.002
2	22	0.4	0.25	0.45	0.15	0.03	0.02	0.005
3	25	0.8	0.5	0.24	0.3	0.03	0.02	0.005
4	18	0.2	0.1	0.12	0.5	0.03	0.02	0.005

under a N_2 protective atmosphere. High-temperature oxidation resistance properties were tested in a muffle furnace; the samples were exposed at 1000 °C for about 10 h and then cooled to room temperature along with the protection of N_2 (for about 2 h). The samples were then exposed to air at room temperature for one night about 12 h. A photoelectric analytical balance (accuracy 0.01 mg) was used to weigh the samples' qualities. The above process was operated cyclically. The oxidized samples were investigated by the use of an X-ray diffractometer (XRD) and a JSM-5800 scanning electron microscope (SEM) was also employed to observe the surface morphology of the oxide scale.

3. Results and discussion

3.1. Thermal expansion properties

Fig. 1 shows the thermal expansion coefficients of the alloys studied. At 900 °C, the thermal expansion coefficient of YSZ was 9.945×10^{-6} cm cm^{-1} K^{-1} while of the four samples were between 11 and 13×10^{-6} cm cm^{-1} K^{-1}. Close to YSZ, the coefficient of Fe-Cr-4 was 11.57×10^{-6} cm cm^{-1} K^{-1}. Compared with traditional alloys (The thermal expansion coefficients of Inconel heat-resistant alloys are bigger than 15×10^{-6} cm cm^{-1} K^{-1}) [17–25], so the new type Fe–Cr based alloys had decreased thermal expansion coefficients.

Thermal stress exists across the interface of the two materials with different thermal expansion properties, such as YSZ and Fe–Cr based alloys, due to their inconsistent shrinkage during cooling. The stress has a direct ratio to the differences in the thermal expansion coefficients between YSZ and Fe–Cr based alloys.

According to Table 2, it is clear that around 500–1000 °C, the differences of the thermal expansion coefficients ($\Delta\alpha$) between YSZ and Fe–Cr based alloys are in the range of $1.1–3.2 \times 10^{-6}$ cm cm^{-1} K^{-1} and the $\Delta\alpha$ range is narrower than that of traditional alloys with the increase of temperature. Besides, the interfacial thermal stress is also decreasing and accordingly the unmatched thermal expansion could be effectively improved.

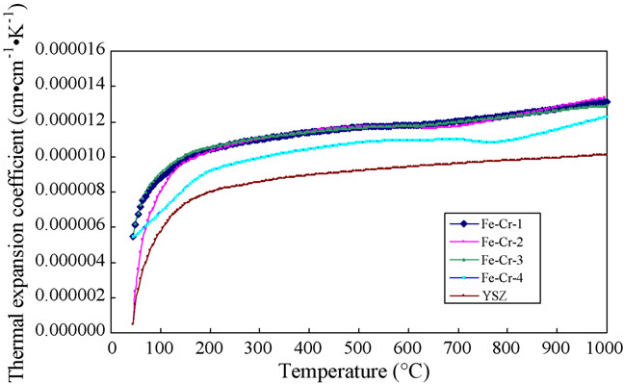

Fig. 1. Comparison of thermal expansion properties between Fe–Cr alloys and YSZ electrolyte.

Small amounts of microelements are helpful to improve the electrical conductivity, heat-resistance and oxidation resistance of the alloys. During the preparation of the materials studied, good heat-resistance and thermal expansion properties depended mainly on Cr and limited amount of Ni (inferior in oxidation resistance). The optimized amount of Cr in this experiment is w(Cr) 18–25% and that of Ni is w(Ni) 0.1–1%.

3.2. Oxidation resistance properties at high temperatures

Weight gain/loss is usually the measurement of the oxidation resistance of heat-resistant alloys. After being oxidized for certain time (t) at certain temperature (1000 °C this experiment), with the protection of N_2, the samples are cooled to room temperature along with the furnace cooling. Then the weight of samples are measured and the unit-area weight gain can be calculated by the following function:

$$y(t) = \frac{W_t - W_0}{S}$$

In this function, W_0, W_t and S, respectively, represent the initial weight, oxidized weight after oxidation for (t) hours and the initial surface areas of the samples.

Weight gain curves of four Fe–Cr alloys after oxidation at 1000 °C for 227 h are given in Fig. 2a, which indicates that Fe-Cr-3 displayed higher weight-gain trends than the other three and exhibits poor oxidation resistance. After oxidation at 1000 °C for 227 h, the weight gain of Fe-Cr-3 was 0.0022 g cm^{-2}, whereas that of Fe-Cr-1 was only 0.0011 g cm^{-2}.

Fig. 2b plots the weight gain curves of these four Fe–Cr alloys after 1-year oxidation in air at room temperature and then 228 h of exposure at 1000 °C. The weight gains of Fe-Cr-1 and -4 after cyclic oxidation for 455 h at 1000 °C were approximately 0.0002 g cm^{-2}, while that of Fe-Cr-3 was still above 0.0005 g cm^{-2} (Fig. 2b). In Fig. 2a and b, the weight gain-oxidation time curves of the alloys exhibit certain curvilinear characters: with the increase of oxidation time, the weight gains of Fe-Cr-1 and -4 tended to be stable.

According to the principles of gas/solid phase reaction kinetics, the alloy oxidation reaction processes are: O_2 (gas phase) diffuses through gas-phase boundary to the surface of oxide then through the oxide scale to the reaction interface; the oxidations are formed on the reaction interface. In the early oxidation stage, the whole reaction speed is mainly controlled by the reaction speed at the interface, since the oxide scale is very thin. In the final stages, it is mainly controlled by diffusion because the O_2 diffusion path widens with the increasing thickness of the scale. While in the middle stage, O_2 diffuses to the interface either through the scale or directly through the oxide scale pores and cracks, so that both the reaction and diffusion speed dominate the oxidation speed.

Table 2
Thermal expansion coefficient differences of Fe–Cr alloys and YSZ electrolyte at different temperatures

	500 °C	600 °C	700 °C	800 °C	900 °C	1000 °C
Thermal expansion coefficient, α ($\times 10^{-6}$ cm cm^{-1} K^{-1})	9.206	9.425	9.618	9.792	9.945	10.11
The difference of thermal expansion coefficient, $\Delta\alpha$ ($\times 10^{-6}$ cm cm^{-1} K^{-1})						
Fe-Cr-1	2.478	2.361	2.402	2.553	2.797	2.974
Fe-Cr-2	2.506	2.296	2.122	2.468	2.883	3.220
Fe-Cr-3	2.469	2.356	2.391	2.517	2.688	2.787
Fe-Cr-4	1.615	1.512	1.396	1.130	1.624	2.134

The oxidation mechanism of Fe–Cr alloys is rather complicated as shown in the above analysis. Its major reaction is the oxidation weight gain of Fe and Cr. The dynamic process of oxidation reaction can be expressed by oxidation functions (Tables 3 and 4) which are obtained from Fig. 2a and b by curve fitting method. Thereinto, y and t, respectively, represent oxidation weight gain and oxidation time.

The XRD patterns of four alloys (Fe-Cr-1–4) in different oxidation conditions are illustrated in Figs. 3–7. The main products obtained were $3Cr_2O_3{\cdot}Fe_2O_3$ and $Cr_2O_3{\cdot}3Fe_2O_3$ after Fe-Cr-1 was oxidized for 20 h at 1000 °C. After 227 h, the oxide consisted of $3Cr_2O_3{\cdot}Fe_2O_3$ and a small amount of $Cr_2O_3{\cdot}3Fe_2O_3$ (Fig. 3).

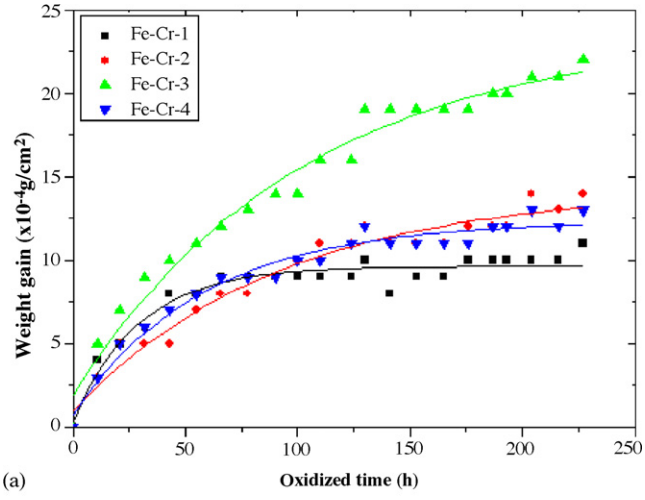

Fig. 2. Weight gain curves of Fe-Cr alloys: (a) oxidized for 227 h at 1000 °C and (b) oxidized 1 year in air, then oxidized for 228 h at 1000 °C.

Table 3
Oxidation functions of Fe–Cr alloys oxidized for 227 h at 1000 °C

Sample	Weight gain (y)—oxidation time (t)
Fe-Cr-1	$\ln[(0.00095 - y)/0.00092] = -0.03601t$
Fe-Cr-2	$\ln[(0.00143 - y)/0.00133] = -0.01080t$
Fe-Cr-3	$\ln[(0.00237 - y)/0.00217] = -0.00971t$
Fe-Cr-4	$\ln[(0.00124 - y)/0.00101] = -0.01733t$

Table 4
Oxidation functions of Fe–Cr alloys oxidized for 228 h at 1000 °C oxidation for 227 h then 1-year oxidation in air

Sample	Weight gain (y)—oxidation time (t)
Fe-Cr-1	$\ln[(0.00027 - y)/0.00029] = -0.01242t$
Fe-Cr-2	$\ln[(0.00064 - y)/0.00061] = -0.00263t$
Fe-Cr-3	$\ln[(0.00178 - y)/0.00177] = -0.00158t$
Fe-Cr-4	$\ln[(0.00020 - y)/0.00021] = -0.04915t$

The major phases of Fe-Cr-2 were $3Cr_2O_3{\cdot}Fe_2O_3$ and $Cr_{1.36}Fe_{0.52}$ after oxidation of 20 h at 1000 °C and only $2Cr_2O_3{\cdot}Fe_2O_3$ was left after oxidation of 227 h as shown in Fig. 4.

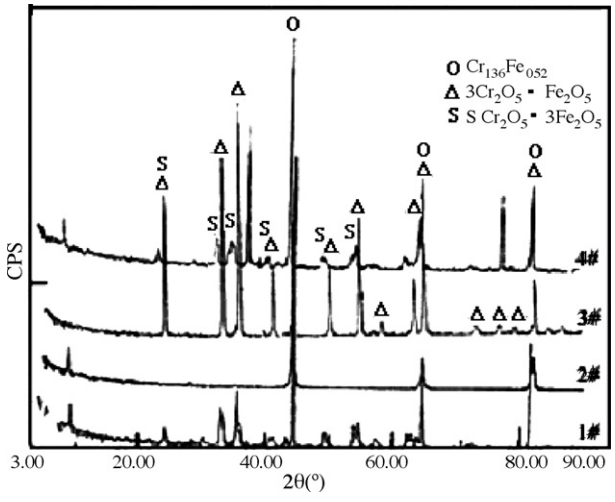

Fig. 3. X-ray diffraction patterns of sample Fe-Cr-1: (1#) raw sample, (2#) polished sample, (3#) sample calcined for 227 h at 1000 °C, and (4#) sample calcined for 20 h at 1000 °C.

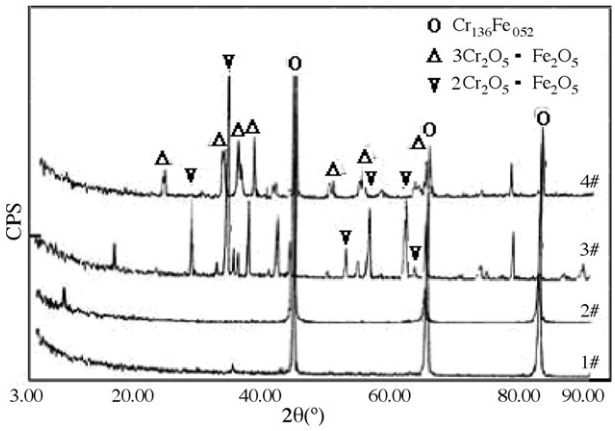

Fig. 4. X-ray diffraction patterns of sample Fe-Cr-2: (1#) raw sample, (2#) polished sample, (3#) sample calcined for 227 h at 1000 °C, and (4#) sample calcined for 20 h at 1000 °C.

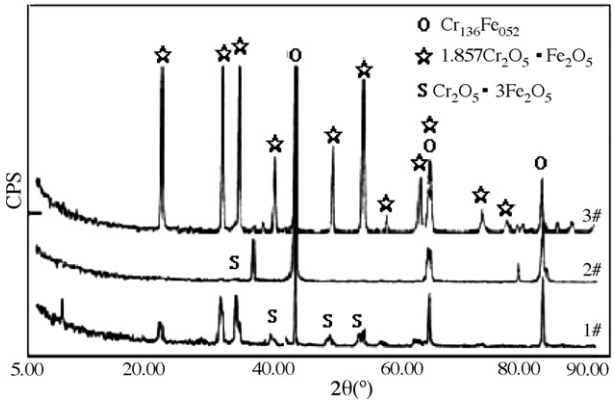

Fig. 5. X-ray diffraction patterns of sample Fe-Cr-3: (1#) raw sample, (2#) polished sample, and (3#) sample calcined for 227 h at 1000 °C.

After 227 h of exposure at 1000 °C, the main product of Fe-Cr-3 was $1.857Cr_2O_3{\cdot}Fe_2O_3$ (Fig. 5) while $3Cr_2O_3{\cdot}Fe_2O_3$ was obtained from Fe-Cr-4 in the same oxidation condition (Fig. 6).

Fig. 7 clearly shows the different surface phase changes of the four sample alloys after oxidation of 227 h at 1000 °C then 1-year of oxidation in air and oxidation of 228 h at 1000 °C.

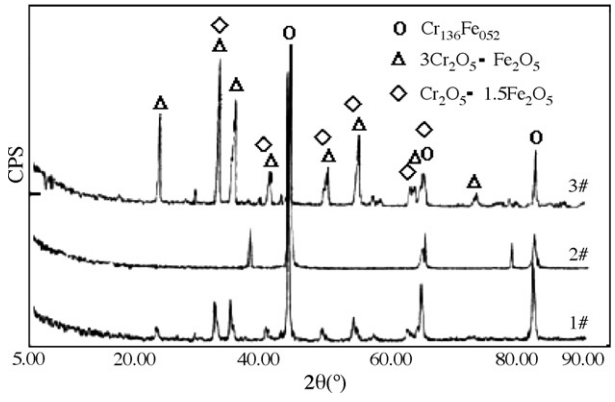

Fig. 6. X-ray diffraction patterns of sample Fe-Cr-4: (1#) raw sample, (2#) polished sample, and (3#) sample calcined for 227 h at 1000 °C.

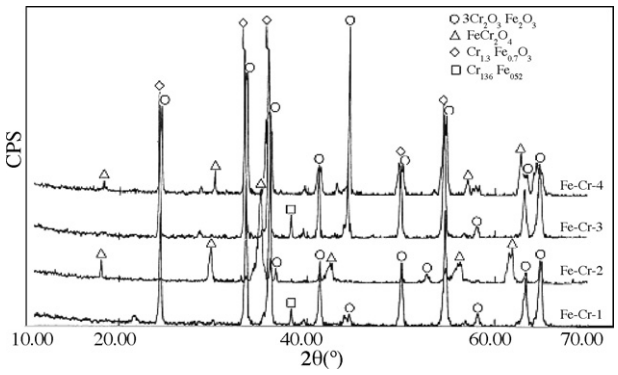

Fig. 7. X-ray diffraction patterns of sample Fe–Cr alloys.

$3Cr_2O_3{\cdot}Fe_2O_3$ was the main product of Fe-Cr-1 and -4. $3Cr_2O_3{\cdot}Fe_2O_3$ and $FeCr_2O_4$ were obtained from Fe-Cr-2. The main product of Fe-Cr-3, different from the other three, was found to be $Cr_{1.3}Fe_{0.7}O_3$.

3.3. Surface morphology

Fig. 8 shows the surface morphology of oxide scale on Fe–Cr alloys after cyclic oxidation for 455 h at 1000 °C. The surface of Fe-Cr-1 was covered with a compact oxide scale consisting of small grains of about 1–2 μm in size and big nodules of about 20 μm in size (Fig. 8a). However, the size of the grains in the big nodules cannot be estimated because they were joined or agglomerated. Grains of about 2–4 μm in size were distributed evenly on the compact oxide scale of Fe-Cr-4, and small grains of about 0.5–1 μm, filling in the gaps among the bigger ones, were observed (Fig. 8d).

Due to the loose and incompact oxide scale, obvious cracks and pores were distinguished on Fe-Cr-2 and -3 (Fig. 8b and c). On the oxide scale of Fe-Cr-2, some cracks stretched to 100 μm and the width of some pores exceeded 2 μm. After longer oxidation times, the outer part of the scale easily peeled off during cooling.

From the above SEM analysis, it can be concluded that at the beginning of oxidation, a discontinuous Cr_2O_3 scale was formed but could not protect the alloy from internal oxidation. At the same time, Fe became enriched and diffused outwards which caused the formation and rapid growth of Fe_2O_3. Blocked by Cr_2O_3, Fe_2O_3 nucleated and grew at the discontinuous areas such as the incompact Cr_2O_3 scale or its micro-defective areas, leading to some bulges and pores. Then, with the outwards diffusion of Cr, a $3Cr_2O_3{\cdot}Fe_2O_3$, scale was developed.

The outer scale was easy to peel off and decomposed during further oxidation. The decomposed product oxygen may diffuse to the oxidation/alloy interface through the cracks and pores in the oxide scale, which led to the formation of an inner oxide scale. That is, the outward diffusion of metallic ions dominated the development of the outer and middle oxide scales, whereas the inner oxide scale was caused by the inward diffusion of oxygen ions. The Cr in Fe-Cr-1, -4 diffused outwards and brought about the formation of stable $3Cr_2O_3{\cdot}Fe_2O_3$ phase; it also filled the gaps with Cr_2O_3-rich scales in areas without Fe_2O_3, which

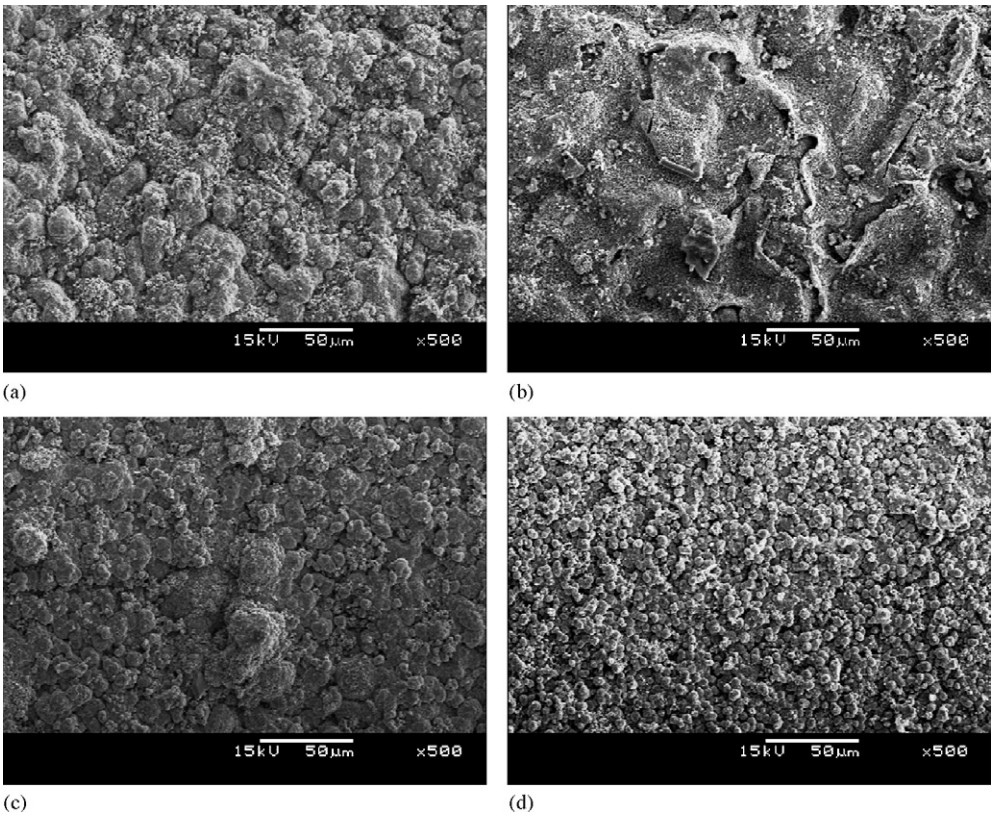

Fig. 8. Micrograph of oxidized scale of Fe–Cr alloys (SEM): (a) Fe-Cr-1, (b) Fe-Cr-2, (c) Fe-Cr-3, and (d) Fe-Cr-4.

blocked the inward diffusion of oxygen and restrained the formation of oxide scale. Thus, Fe-Cr-1 and -4 exhibit better oxidation resistance. As to Fe-Cr-2 and -3, their poor oxidation resistance might be related to the additional microelements which obstructed the outward diffusion of Cr and hindered the formation of compact and stable $3Cr_2O_3{\cdot}Fe_2O_3$. Further research is needed on the effect of the additional microelements to high temperature oxidation.

In the initial oxidation stage, the proportion of Cr and Fe in the oxide scale was similar to that in the alloys; after longer oxidation times, Cr continuously diffused and agglomerated towards the scale surface, then part of it directly oxidized with O and partly substituted the Fe in Fe_2O_3. This conclusion could be clearly proven by the XRD patterns from Figs. 5–8 which plotted the increase of $3Cr_2O_3{\cdot}Fe_2O_3$ and decrease of $Cr_2O_3{\cdot}3Fe_2O_3$.

4. Conclusions

At 900 °C, the thermal expansion coefficients of the four samples studied were between 11 and 13×10^{-6} cm cm^{-1} K^{-1}. The coefficient of sample Fe-Cr-4 was closest to that of yttrium stabilized zirconia (YSZ). Compared with traditional alloys, the new type Fe–Cr based alloys had decreased thermal expansion coefficients.

The weight gain/oxidation time curves of the alloys exhibited certain curvilinear characteristics: with increase of oxidation time, the weight gains of Fe-Cr-1 and -4 tended to be stable. Studies of the oxidation resistance of Fe–Cr based alloys showed significant differences. The oxide scale of $3Cr_2O_3{\cdot}Fe_2O_3$ formed on the surface of Fe-Cr-1 and -4 was inactive and helpful in restraining internal oxidation. But the $FeCr_2O_4$ and $Cr_{1.3}Fe_{0.7}O_3$ formed on the surface of Fe-Cr-2 and -3 had no such effective restraint on internal oxidation. Fe-Cr-1 and -4 exhibited much better oxidation resistance than Fe-Cr-2 and -3.

Acknowledgements

We would like to thank China National Ministry of Education Key Project Foundation for financial support with contract 106087, and China National High-tech 863 Project Foundation for financial support with contract 2005AA501050.

References

[1] F.J. Gardner, M.J. Day, J. Power Sources 86 (2000) 122.
[2] S. Peng, M. Han, C. Yang, J. Phys. 33 (2004) 90 (in Chinese).
[3] S.T. Aruna, M. Muthuraman, K.C. Patil, Solid State Ionics 111 (1998) 45.
[4] T.-L. Wen, D. Wang, M. Chen, H. Tu, Z. Lu, Z. Zhang, H. Nie, W. Huang, Solid State Ionics 148 (2002) 513.
[5] J.-H. Lee, J.-W. Heo, D.-S. Lee, J. Kim, G.-H. Kim, H.-W. Lee, H.S. Song, J.-H. Moon, Solid State Ionics 158 (2003) 225.
[6] S. Primdahl, M. Mogensen, J. Electrochem. Soc. 146 (1999) 2827.
[7] M. Brown, S. Primdahl, M. Mogensen, J. Electrochem. Soc. 147 (2000) 475.
[8] K. Hilpert, R.W. Steinbrech, F. Boroomand, J. Eur. Ceram. Soc. 23 (2003) 3009.
[9] W.Z. Zhu, S.C. Deevi, Mater. Sci. Eng. A 348 (2003) 227.

[10] M. Mori, Y. Hiei, J. Am. Ceram. Soc. 84 (2001) 2573.
[11] N.M. Sammes, R. Ratnaraj, J. Mater. Sci. 30 (1995) 4523.
[12] S.P. Simner, J.S. Hardy, J.W. Stevenson, T.R. Armstrong, Solid State Ionics 128 (2000) 53.
[13] Z.G. Yang, M. Walker, G. Xia, P. Singh, J. Stevenson, SECA CTP Review Meeting, Albany, NY, September 30, 2003.
[14] N. Dekker, B. Rietveld (ECN), J. Laatsch, F. Tietz, Proceedings of the Sixth European Solid Oxide Fuel Cell Forum, June 28–July 2, 2004, p. 319.
[15] H. Teruhisa, X. Yueping, Y. Katsuhiko, J. Electrochem. Soc. 150 (2003) A243.
[16] M. Han, S. Peng, Patent No. CN 1468970A, Zl 02 1 55409.9, 2002 (in Chinese).
[17] D.M. England, A.V. Virkar, J. Electrochem. Soc. 146 (9) (1999) 3196–3202.
[18] D.M. England, A.V. Virkar, J. Electrochem. Soc. 148 (4) (2001) A330–A338.
[19] A.V. Virkar, D.M. England, US Patent 6054231, 2000.
[20] Y. Miyake, T. Yasuo, Y. Akiyama, S. Taniguchi, M. Kadowaki, H. Kawamura, T. Saitoh, in: M. Dokiya, O. Yamamoto, H. Tagawa, S.C. Singhal (Eds.), Solid Oxide Fuel Cell IV, The Electrochemical Society Proceedings, PV95-1, Pennington, NJ, 1995, p. 100.
[21] T. Iwata, N. Kadokawa, S. Takenoiri, in: M. Dokiya, O. Yamamoto, H. Tagawa, S.C. Singhal (Eds.), Solid Oxide Fuel Cell IV, The Electrochemical Society Proceedings, PV95-1, Pennington, NJ, 1995, p. 110.
[22] T. Shiomitsu, T. Kadowaki, I. Ogawa, T. Maruyama, in: M. Dokiya, O. Yamamoto, H. Tagawa, S.C. Singhal (Eds.), Solid Oxide Fuel Cell IV, The Electrochemical Society Proceedings, PV95-1, Pennington, NJ, 1995, p. 850.
[23] S.P.S. Badwal, R. Deller, K. Foger, Y. Ramprakash, J.P. Zhang, Solid State Ionics 99 (1997) 297–310.
[24] Y. Matsuzaki, I. Yasuda, Solid State Ionics 132 (2000) 271–278.
[25] T. Malkow, W.J. Quadakkers, L. Singheiser, H. Nickel, Report Forschungszenttum Julich, Julich, FRG, Jul-3589, 1998, ISSN 1944-2952.